A Variable Rate Supertwisting Sliding Mode Speed Control With Overcurrent Protection for PMSM Considering Aperiodic and Periodic Disturbances

Yongzhi Chen and Xudong Liu

***Abstract*—Aiming at improving the speed regulation performance of permanent magnet synchronous motor (PMSM) under aperiodic and periodic disturbances, a variable rate supertwisting (VRST) sliding mode control strategy based on a novel disturbance observer (NDO) is proposed in this article considering overcurrent protection. First, the model of PMSM considering aperiodic disturbances and periodic harmonic disturbances is established. Second, to enhance the antidisturbance performance and the control accuracy, an NDO is designed to estimate periodic harmonic disturbances and aperiodic disturbances, such as load torque, parameter uncertainties. Furthermore, the variable rate nonlinear term is introduced into the supertwisting sliding mode control algorithm, and a VRST sliding mode single-loop speed controller is proposed to improve the transient performance. Meanwhile, an improved q-axis current penalty function is designed to avoid excessive current, which can effectively balance dynamic performance and overcurrent protection. Subsequently, based on the Lyapunov theory, the stability of the control system is analyzed. Finally, the superiority and effectiveness of the proposed control scheme are verified through a series of comparative experiments.**

***Index Terms*—Harmonic disturbances, overcurrent protection, penalty function, permanent magnet synchronous motor (PMSM), single-loop control, variable rate supertwisting (VRST).**

I. Introduction

PERMANENT magnet synchronous motors (PMSMs) not only have the superiorities of high efficiency, high power density, and low noise vibration, but also have a simple and reliable structure. Therefore, they are widely used in electric vehicles [1], high-precision machine tools [2], electric aircraft [3], and other fields. However, the traditional proportional–integral (PI) control cannot satisfy the control requirements of these fields. Nowadays, with the development of nonlinear theory, computer control technology, and modern power electronics, some advanced nonlinear algorithms, such as robust control [4], active disturbance rejection control [5], model predictive control [6], fuzzy control [7], adaptive control [6], and sliding mode control (SMC) [8], have been applied to motor drive systems. Thus, the control performance in motors is improved.

Among these methods, SMC has the features of simple structure, strong robustness for the disturbances and fast response, therefore, it is widely used in motor drives [9], [10]. Nevertheless, the conventional SMC is not flawless. In practical applications, the chattering is inevitable due to the presence of signum function in controller. Hence, reducing chattering is crucial in SMC. At present, several methods have been proposed to mitigate the chattering phenomenon, such as fractional-order SMC [11], high-order SMC [12], variable gain SMC [13]. They effectively reduced chattering, but the response time may be increased. The fast-reaching law method is usually applied to reduce the convergence time since it is simple to be designed. In order to accelerate the convergence speed, a hybrid reaching law [14] composed of terminal terms and proportional terms is proposed. To further improve dynamic performance, a sliding mode speed controller with an adaptive reaching law [15] is proposed for the control of PMSM, which shortens the convergence time. A supertwisting sliding mode control (STSMC) algorithm is proposed in [16], the discontinuous signum function is hidden in integral term, and the global finite-time convergence is achieved. In [17], the STSMC algorithm is applied to the isolated dc–dc power converter, the voltage tracking performance and voltage stability is improved. To further improve dynamic performance and reduce overshoot. Zhen et al. [18] presented an adaptive supertwisting sliding control to ensure the rapidity and robustness of carrier autolanding system. A sliding mode composite control based on improved supertwisting is proposed in [19] by adding terminal term to accelerate convergence speed, and estimated peak value is reduced via a time-varying disturbance observer. In [20], the parameters range of the supertwisting algorithm is given by analyzing the stability with Lyapunov function, and the convergence time was calculated.

As is known to all, SMC methods have a good suppression effect on matched disturbances. However, the single-loop speed control system of PMSM is susceptible to mismatched disturbance [21]. The common solution is to design mismatched disturbance observers for feedforward compensation of the controller, such as extended state observer [22], nonlinear

Received 19 June 2024; revised 24 October 2024; accepted 6 December 2024. Date of publication 11 December 2024; date of current version 28 January 2025. This work was supported in part by the National Natural Science Foundation of China under Grant 62473218 and Grant 62273189, in part by the Shandong Provincial Natural Science Foundation under Grant ZR2022MF262 and Grant ZR2021MF005, and in part by the Systems Science Plus Joint Research Program of Qingdao University under Grant XT2024201. Recommended for publication by Associate Editor S.-C. Yang. *(Corresponding author: Xudong Liu.)*

The authors are with the School of Automation, Qingdao University, the Key Laboratory of Industrial Control Technology, Qingdao 266071, China (e-mail: chenyongzhi@qdu.edu.cn; lxd2017@qdu.edu.cn).

Color versions of one or more figures in this article are available at https://doi.org/10.1109/TPEL.2024.3515086.

Digital Object Identifier 10.1109/TPEL.2024.3515086

disturbance observer [23], and sliding mode observer [24]. They have a good effect on estimating aperiodic disturbance. However, the performance of the speed control is also affected by periodic disturbances, such as torque ripple caused by current sampling error, which produce severe speed fluctuations. In recent years, some methods have been studied to suppress periodic disturbances, mainly including internal model control and feedforward estimation compensation. In [25], an active disturbance rejection controller (ADRC) is combined with a quasiresonant controller (QRC) to suppress both periodic and aperiodic disturbances. However, the QRC is susceptible to aperiodic disturbances, which can reliable and stable operation only by limiting the load torque. Repetitive controller is embedded in ADRC to compensate for alternating current disturbance of current-loop in [26], which is not suitable for speed-loop because some periodic signals may be amplified. In [27], an iterative learning control method is proposed to suppress position harmonic error. All the above-mentioned methods belong to internal model control. In addition, some intelligent algorithms such as neural network [28] are proposed to suppress current harmonics. However, these methods require complex calculations.

In addition, compared with the conventional cascade control structure for motor drive, the q-axial current in noncascade control cannot be regulated by the desired signal. Therefore, overcurrent protection becomes an important issue. Recently, state constraint control methods based on penalty function have been proposed. In [29], [30], and [31], a q-axis current penalty function is added to the controller, and the current is constrained within a safe range. Moreover, a transformation scheme [32] is proposed to balance control performance and overcurrent protection. However, the derivation of the sliding mode controller becomes extremely complex.

In this article, a variable rate supertwisting (VRST) SMC strategy based on an NDO is proposed to further improve the speed control performance of PMSM. Compared with former works, the contributions and novelties of this article are as follows.

1) A variable rate nonlinear term is introduced into the supertwisting algorithm, and a VRST sliding mode single-loop controller is proposed to accelerate the convergence of the system.
2) To enhance the speed tracking accuracy and reduce speed fluctuations of PMSM, a novel disturbance observer (NDO) is proposed to estimate aperiodic disturbances and periodic harmonic disturbances simultaneously.
3) An improved q-axis current penalty function is designed to balance dynamic performance and overcurrent protection.
4) A series of experimental tests are conducted on the PMSM RT-SIM experimental platform to verify the effectiveness of the proposed control strategy, and the superiority of the proposed control method is verified through comparative experiments.

The rest of this article is organized as follows. The model of PMSM considering aperiodic and periodic disturbances is described in Section II. In Section III, the NDO is designed to estimate the disturbances in single-loop control of PMSM. Section IV presents a VRST sliding mode speed controller and the analysis of system stability is completed. In Section V, the experiments are conducted to validate the effectiveness and superiority of the proposed strategy. Finally, Section VI concludes this article.

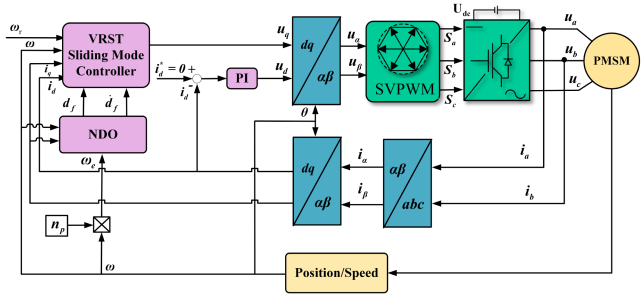

Fig. 1. Single-loop structure diagram with the proposed SMC and NDO in PMSM.

II. Model Description of PMSM

According to field-oriented control theory, the mathematical model of PMSM in d-q axis rotational coordinate can be established as

$$\begin{cases} \frac{\mathrm{d}i_\mathrm{d}}{\mathrm{d}t} = -\frac{R_\mathrm{s}}{L_\mathrm{d}} i_\mathrm{d} + \frac{n_\mathrm{p}\omega L_\mathrm{q}}{L_\mathrm{d}} i_\mathrm{q} + \frac{1}{L_\mathrm{d}} u_\mathrm{d} \\ \frac{\mathrm{d}i_\mathrm{q}}{\mathrm{d}t} = -\frac{R_\mathrm{s}}{L_\mathrm{q}} i_\mathrm{q} - \frac{n_\mathrm{p}\omega L_\mathrm{d}}{L_\mathrm{q}} i_\mathrm{d} - \frac{n_\mathrm{p}\Phi}{L_\mathrm{q}}\omega + \frac{1}{L_\mathrm{q}} u_\mathrm{q} \\ \frac{\mathrm{d}\omega}{\mathrm{d}t} = \frac{T_\mathrm{e}}{J} - \frac{B}{J}\omega + f_\omega \end{cases} \tag{1}$$

where L_d and L_q are the d-q axis stator inductances, respectively. i_d, i_q and u_d, u_q indicate the d-q stator current and stator voltage, respectively. ω is the mechanical angular velocity. T_e is the electromagnetic torque. J is the rotational inertia. R_s indicates stator resistance. B is viscous friction coefficient. Φ is the permanent magnet flux. n_p is pole pairs. f_ω is the aperiodic and periodic disturbances.

The electromagnetic torque T_e is expressed as

$$T_\mathrm{e} = n_\mathrm{p}\left[\Phi i_\mathrm{q} + \left(L_\mathrm{d} - L_\mathrm{q}\right) i_\mathrm{d} i_\mathrm{q}\right]. \tag{2}$$

For surface-mounted PMSM, due to $L_\mathrm{q} = L_\mathrm{d}$, the mechanical motion equation in (1) can be simplified as

$$\frac{\mathrm{d}\omega}{\mathrm{d}t} = \frac{n_\mathrm{p}\Phi i_\mathrm{q}}{J} - \frac{B}{J}\omega + f_\omega. \tag{3}$$

Usually, the speed control system of PMSM consists of a speed-loop and a current-loop with a cascade configuration, and the speed is usually regulated by PI controller. To make the controller structure simplification and reduce the difficulty of parameter adjustment, a VRST sliding mode single-loop controller is proposed for the speed control of PMSM. Meanwhile, an NDO is designed to estimate the aperiodic and periodic disturbances of the system, and it is used for the feedforward compensation of the controller. The overall structural diagram of PMSM speed control system is shown in in Fig. 1.

In practical systems, the lumped disturbances are inevitable, which include aperiodic disturbance and periodic harmonic disturbances. Among them, periodic harmonic disturbances in PMSM mainly caused by flux harmonics, voltage harmonics,

and current sampling errors. The flux harmonics and voltage harmonics caused by inverter nonlinearity are relatively small [33]. Therefore, the periodic disturbances arise from current sampling error is mainly considered in this article. The offset error and scaling error are components of the current sampling error, which will produce first and second speed harmonics in the *d-q* axis coordinates [34].

Based on the above-mentioned analysis, f_ω can be specifically defined as $f_\omega = -T_{\rm L}/J - T_{\rm h1}/J - T_{\rm h2}/J$. $T_{\rm L}$ is load torque. $T_{\rm h1}, T_{\rm h2}$ are the first and second torque ripple caused by current sampling error.

To achieve the accuracy speed regulation with single-loop structure, choose the state variables as $x = [x_1 \quad x_2] = [e_\omega \quad -(n_{\rm p}\Phi/J)i_{\rm q}]$, where $e_\omega = \omega_{\rm r} - \omega$ is the speed tracking error, and $\omega_{\rm r}$ is the reference speed. Then, a state space model considering aperiodic disturbances and periodic disturbances can be described as

$$\begin{cases} \dot{x}_1 = \dot{\omega}_{\rm r} - \frac{n_{\rm p}\Phi}{J} i_{\rm q} + \frac{B}{J}\omega - f_\omega = x_2 + d + d_{\rm h1} + d_{\rm h2} \\ \dot{d}_{\rm h1} = z_1,\ \dot{z}_1 = -\omega_{\rm e}^2 d_{\rm h1} \\ \dot{d}_{\rm h2} = z_2,\ \dot{z}_2 = -4\omega_{\rm e}^2 d_{\rm h2} \\ \dot{x}_2 = -\frac{n_{\rm p}\Phi}{J}\dot{i}_{\rm q} = a(x) + bu_{\rm q} \end{cases} \tag{4}$$

where d represents the aperiodic disturbance, $d = \dot{\omega}_{\rm r} + (B/J)\omega + T_{\rm L}/J$. $d_{\rm h1} = T_{\rm h1}/J = H_1 \sin(\omega_{\rm e} t + \varphi_1)$, $d_{\rm h2} = T_{\rm h2}/J = H_2 \sin(2\omega_{\rm e} t + \varphi_2)$ are first and second harmonic disturbances, respectively. H_1, H_2 and φ_1, φ_2 are the unknown amplitudes and the unknown phases, respectively. z_1, z_2 are intermediate variables, $\omega_{\rm e} = n_{\rm p}\omega$ is electric angular velocity,, $a(x) = n_{\rm p}\Phi(R_{\rm s} i_{\rm q} + n_{\rm p}\omega L_{\rm d} i_{\rm d} + n_{\rm p}\omega\Phi)/(JL_{\rm q})$, $b = -(n_{\rm p}\Phi)/JL_{\rm q}$.

III. Design of NDO

To enhance antidisturbance performance and control accuracy of PMSM caused by lumped disturbances, an NDO is designed to estimate the slow-varying aperiodic disturbances and the periodic harmonic disturbances simultaneously.

Assumption 1: The aperiodic disturbance d and its derivative $\dot{d}$ are both bounded, that is, $|d| \le D_1$, $|\dot{d}| \approx 0$, D_1 is positive constant [35]. Obviously, the first and second harmonic disturbances $d_{\rm h1}$, $d_{\rm h2}$ with their *n*-order derivatives are bounded.

Lemma 1: [36] Consider the system (5), $(x_1, x_2, \cdots, x_n) \in \mathbb{R}^n$ are system states, $u \in \mathbb{R}$ is control input, $y \in \mathbb{R}$ is system output

$$\begin{cases} \dot{x}_j = x_{j+1} \\ \dot{x}_n = u \quad j = 1, 2, \ldots, n-1 \\ y = x_1. \end{cases} \tag{5}$$

For any $\Lambda \in (-1/n, 0)$, there exit constant gains l_j such that the states $(\hat{x}_1, \hat{x}_2, \ldots, \hat{x}_n)$ of the observer (6) converge to the real states $(x_1, x_2, \ldots, x_n)$ in a finite time

$$\begin{cases} \dot{\hat{x}}_j = \hat{x}_{j+1} + l_j {\rm sig}^{j\Lambda+1}(x_1 - \hat{x}_1) \\ \qquad\qquad j = 1, 2, \ldots, n-1 \\ \dot{\hat{x}}_n = u + l_n {\rm sig}^{n\Lambda+1}(x_1 - \hat{x}_1). \end{cases} \tag{6}$$

For periodic disturbances, the designed principle in this article is based on the property that the second derivative of a sine signal has a specific multiple relationship with its own. Then, inspired by Huang et al. [37], an NDO with the following structure is designed as:

$$\begin{cases} \dot{\hat{x}}_1 = x_2 + \hat{d} + \hat{d}_{\rm h1} + \hat{d}_{\rm h2} + l_1 {\rm sig}^{\alpha_1}(x_1 - \hat{x}_1) \\ \dot{\hat{d}} = l_2 {\rm sig}^{\alpha_2}(x_1 - \hat{x}_1) \\ \dot{\hat{d}}_{\rm h1} = \hat{z}_1 + l_3 {\rm sig}^{\alpha_3}(x_1 - \hat{x}_1) \\ \dot{\hat{z}}_1 = -\omega_{\rm e}^2 \hat{d}_{\rm h1} + l_4 {\rm sig}^{\alpha_4}(x_1 - \hat{x}_1) \\ \dot{\hat{d}}_{\rm h2} = \hat{z}_2 + l_5 {\rm sig}^{\alpha_5}(x_1 - \hat{x}_1) \\ \dot{\hat{z}}_2 = -4\omega_{\rm e}^2 \hat{d}_{\rm h2} + l_6 {\rm sig}^{\alpha_6}(x_1 - \hat{x}_1) \end{cases} \tag{7}$$

where $\hat{x}_1, \hat{d}, \hat{d}_{\rm h1}, \hat{d}_{\rm h2}, \hat{z}_1$, and $\hat{z}_2$ are the estimation of $x_1, d, d_{\rm h1}, d_{\rm h2}, z_1$, and z_2. $l_i > 0, (i = 1, 2, \ldots, 6)$ are gains of observer. ${\rm sig}^{\alpha_i}(\cdot) = |\cdot|^{\alpha_i}{\rm sign}(\cdot)$, $\alpha_i \in (0, 1)$, $(i = 1, 2, \ldots, 6)$.

According to [37] and [38], the observer gains l_i can be tuned by bandwidth parametrization method. First, define the observer bandwidth as ω_0. Subsequently, the characteristic polynomial can be derived as $s^2 + l_i s + l_{i+1} = (s + \omega_0)^2$, $i = (1, 3, 5)$. $l_i = 2\omega_0$, $l_{i+1} = \omega_0^2$. The convergence rate of NDO will be affected by ω_0. The larger the ω_0 is, the faster the convergence speed is. However, excessively large ω_0 will amplify the high-frequency noise and reduce estimation accuracy. Therefore, it is crucial to make a tradeoff between convergence rate and estimation accuracy. Then, according to lemma 1, for the designed NDO, the system order $n = 2$, and $\alpha_i \in (0.5, 1)$, $\alpha_{i+1} \in (0, 1)$. According to [39], these parameters should be selected to be close to 1 to achieve highly accurate estimation of disturbances and strong robustness. If these parameters are far from 1, the dynamic performance of the observer will be affected.

Define the estimation error variables as

$$\begin{cases} e_1 = x_1 - \hat{x}_1 \\ e_2 = d - \hat{d} \\ e_3 = d_{\rm h1} - \hat{d}_{\rm h1} \\ e_4 = z_1 - \hat{z}_1 \\ e_5 = d_{\rm h2} - \hat{d}_{\rm h2} \\ e_6 = z_2 - \hat{z}_2. \end{cases} \tag{8}$$

By combining the established model (4) and observer (7), the derivative of (8) is obtained as

$$\begin{cases} \dot{e}_1 = e_2 + e_3 + e_5 - l_1 {\rm sig}^{\alpha_1}(e_1) \\ \dot{e}_2 = -l_2 {\rm sig}^{\alpha_2}(e_1) \\ l\dot{e}_3 = e_4 - l_3 {\rm sig}^{\alpha_3}(e_1) \\ \dot{e}_4 = -\omega_{\rm e}^2 e_3 - l_4 {\rm sig}^{\alpha_4}(e_1) \\ \dot{e}_5 = e_6 - l_5 {\rm sig}^{\alpha_5}(e_1) \\ \dot{e}_6 = -4\omega_{\rm e}^2 e_5 - l_6 {\rm sig}^{\alpha_6}(e_1). \end{cases} \tag{9}$$

According to Assumption 1 and Lemma 1, it can be concluded that the states errors of system (9) can converge to the origin in a finite time.

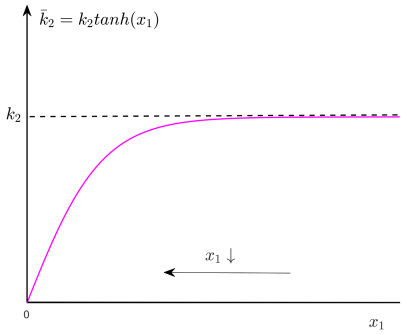

Fig. 2. Variation of gain $\bar{k}_2 = k_2 \tanh(|x_1|^{c_1}), c_1 = 1$.

IV. Design of VRST Sliding Mode Controller

A. VRST Control Law

To accelerate convergence rate while ensuring the minimal chattering, a VRST control law with variable gain and variable power nonlinear term is designed as

$$\begin{aligned} \dot{s} &= -k_1 \mathrm{sig}^{1/2}(s) - \bar{k}_2 \mathrm{sig}^{r}(s) + g \\ \dot{g} &= -k_3 \mathrm{sign}(s) \end{aligned} \tag{10}$$

where $\mathrm{sig}^{1/2}(s) = |s|^{1/2}\mathrm{sign}(s)$, $\mathrm{sig}^{r}(s) = |s|^{r}\mathrm{sign}(s)$. The variable power $r = 1 - r_1 \mathrm{sign}(1 - |s|)$ varies with the value of $|s|$, $0 < r_1 < 1$. $\mathrm{sign}(\cdot)$ is the signum function. The variable gain $\bar{k}_2 = k_2 \tan \mathrm{h}(|x_1|^{c_1})$, $c_1 > 0$, $\tanh(\cdot)$ is the hyperbolic tangent function. x_1 is the state variable. $k_i > 0$ $(i = 1, 2, 3)$ are constants to be designed.

Compared with the existing supertwisting control [17], a variable rate nonlinear term is introduced into the proposed supertwisting algorithm. If the convergence space of sliding mode variable is divided into $[0, 1]$ and $[1, \infty]$, the parameter r is equivalent to $r = 1 - r_1$ and $r = 1 + r_1$, respectively. Thus, $\mathrm{sig}^{r}(s)$ has a larger value than s throughout the entire approaching process, and the faster convergence speed can be obtained. In addition, the gain $\bar{k}_2$ is related to the state variable x_1 (speed tracking error), and its value varies with x_1 as shown in Fig. 2. It can be seen that as x_1 changes, $\bar{k}_2$ varies from k_2 to 0. When the state variable x_1 gradually converges to the domain of zero along the sliding mode surface, the gain $\bar{k}_2$ will quickly decrease, and the chattering can be effectively suppressed.

In summary, the variable rate nonlinear term $\bar{k}_2 \mathrm{sig}^{r}(s)$ plays an important role in accelerating convergence speed when the system state is far from the sliding surface (approaching process). When the state variable slides on the sliding surface (sliding process), the values of $\bar{k}_2$ will decrease, and the sliding mode chattering will be further reduced.

B. Improved Q-Axis Current Penalty Function

The q-axial current in single-loop control structure cannot be regulated by the reference current signal, and the current cannot be guaranteed to be within a safe range. Therefore, the potential hazard caused by excessive currents cannot be ignored. Originally, the traditional approach is to select conservative parameters, but the dynamic performance of the controller will inevitably be affected. To balance overcurrent protection and dynamic performance well, a piecewise continuous current penalty function is designed as $1/\delta(\kappa)$, where

$$\delta(\kappa) = \begin{cases} 1 & ,\eta < \kappa \\ 1 - \varepsilon(\frac{\kappa}{\eta} - 1)^2 & ,0 < \kappa \le \eta \\ \bar{\varepsilon} & ,\kappa \le 0 \end{cases}$$

$\bar{\varepsilon} = 1 - \varepsilon$. $\kappa = \varsigma^2 - i_{\mathrm{q}}^2$, ς is the boundary value for the overcurrent protection to be designed, i.e., $i_{\mathrm{q}}(t) \in (-\varsigma, \varsigma)$. $\eta \in (0, \varsigma^2)$ is a threshold value for switching when the current constraints conditions are met.

Remark 1: The penalty function is an additional term related to a restricted variable, which can forcibly constrain the variable within a predetermined range. If $\eta < \kappa$, the penalty term has no effect on the dynamic performance and antidisturbance performance of the controller. If $0 < \kappa \le \eta$, the current i_q approaches the predetermined boundary value, in this case, the penalty function will play a role in the designed controller to prevent excessive current. If $\kappa < 0$, $\bar{\varepsilon}$ is designed to avoid the negative impacts of penalty function on the system.

C. Design of Sliding Mode Single-Loop Speed Controller

According to the established model (4), a VRST sliding mode single-loop controller will be designed. In addition, an improved penalty function-based q-axis current constraints mechanism will be introduced into the speed error differential gain [30], [31], [40] of the controller. Consider the overcurrent, a nonsingular integral sliding mode surface is proposed as

$$s = x_2 + d_f + \frac{\lambda_0}{\delta(\kappa)} x_1 + \lambda_1 \int_0^t \mathrm{sig}^{p}(x_1)\, d\tau \tag{11}$$

where $\lambda_i > 0\,(i = 0, 1), p > 0$ are the parameters to be selected. $\lambda_0/\delta(\kappa)$ is considered as a control gain. $d_f = \hat{d} + \hat{d}_{\mathrm{h1}} + \hat{d}_{\mathrm{h2}}$, $\hat{d}, \hat{d}_{\mathrm{h1}}$, and $\hat{d}_{\mathrm{h2}}$ are the estimated values of d, d_{h1}, and d_{h2}, respectively. $\mathrm{sig}^{p}(x_1) = |x_1|^{p}\mathrm{sign}(x_1)$.

Taking the derivative of (11) yields

$$\dot{s} = \dot{x}_2 + \dot{d}_f + \frac{\lambda_0}{\delta(\kappa)} \dot{x}_1 + \lambda_1 \mathrm{sig}^{p}(x_1). \tag{12}$$

Then, according to the proposed VRST control law (10) and (12). A sliding mode single-loop controller considering q-axis current constraints can be designed as (13), and Fig. 3 shows the structure diagram of VRST sliding mode controller

$$\begin{aligned} u_q &= -\frac{1}{b}\begin{bmatrix} a(x) + \dot{d}_f + \frac{\lambda_0}{\delta(\kappa)}(x_2 + d_f) - g \\ +\lambda_1 \mathrm{sig}^{p}(x_1) + k_1 \mathrm{sig}^{1/2}(s) + \bar{k}_2 \mathrm{sig}^{r}(s) \end{bmatrix} \\ \dot{g} &= -k_3 \mathrm{sign}(s). \end{aligned} \tag{13}$$

Remark 2: When the current i_q approaches the boundary value, i.e., the $0 < \kappa \le \eta$ is satisfied. Then, the gain of $\lambda/\delta(\kappa)$ is automatically increased. In this way, the output of the controller (13) will be adjusted to restrict the current in time.

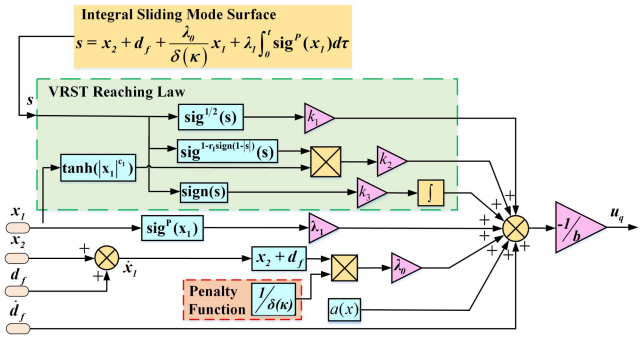

Fig. 3. Structure block diagram of VRST sliding mode controller.

D. Stability Analysis

Substituting the proposed controller (13) into (12) yields

$$\begin{cases} \dot{s} = -k_1 \mathrm{sig}^{1/2}(s) - \bar{k}_2 \mathrm{sig}^{r}(s) + g \\ \quad\quad +\lambda_0 \left(e_2 + e_3 + e_5\right)/\delta\left(\kappa\right) \\ \dot{g} = -k_3 \mathrm{sign}(s) \end{cases} \tag{14}$$

where $e_2 = d - \hat{d}$, $e_3 = d_{\mathrm{h}1} - \hat{d}_{\mathrm{h}1}$, $e_5 = d_{\mathrm{h}2} - \hat{d}_{\mathrm{h}2}$ are disturbance estimation errors.

To facilitate the stability analysis of the controller, define $f(t) = \lambda_0(e_2 + e_3 + e_5)/\delta(\kappa)$. Then, the (14) can be rewritten as

$$\begin{cases} \dot{s} = -k_1 \mathrm{sig}^{1/2}(s) - \bar{k}_2 \mathrm{sig}^{r}(s) + g \\ \dot{g} = -k_3 \mathrm{sign}(s) + \dot{f}(t). \end{cases} \tag{15}$$

Define the Lyapunov function [41] as

$$V = V_1 + V_2 = \zeta_1^{\mathrm{T}} H_1 \zeta_1 + \zeta_2^{\mathrm{T}} H_2 \zeta_2 \tag{16}$$

where $H_1,\ H_2 \in \mathbb{R}^{2\times 2} > 0$, and ζ_1, ζ_2 are determined as

$$\zeta_1 = \begin{bmatrix} \mathrm{sig}^{1/2}(s) \\ g \end{bmatrix},\ \zeta_2 = \begin{bmatrix} \mathrm{sig}^{r}(s) \\ g \end{bmatrix}. \tag{17}$$

After that, the following Rayleigh's inequality can be obtained as:

$$\begin{aligned} \rho_{\min}\left\{H_1\right\} \left\|\zeta_1\right\|^2 \le V_1 \le \rho_{\max}\left\{H_1\right\} \left\|\zeta_1\right\|^2 \\ \rho_{\min}\left\{H_2\right\} \left\|\zeta_2\right\|^2 \le V_2 \le \rho_{\max}\left\{H_2\right\} \left\|\zeta_2\right\|^2 \end{aligned} \tag{18}$$

where $\|\zeta_1\|^2 = |s| + g^2$, $\|\zeta_2\|^2 = |s|^{2r} + g^2$. $\rho_{\min}\{H_1\}$, $\rho_{\min}\{H_2\}$ and $\rho_{\max}\{H_1\}$, $\rho_{\max}\{H_2\}$ denote minimum and maximum eigenvalues of matrix H_1, H_2, respectively.

Taking the derivative of ζ_1 and ζ_2 as

$$\dot{\zeta}_1 = \begin{bmatrix} \frac{1}{2}\left|s\right|^{-\frac{1}{2}} \dot{s} \\ \dot{g} \end{bmatrix},\ \dot{\zeta}_2 = \begin{bmatrix} r\left|s\right|^{r-1} \dot{s} \\ \dot{g} \end{bmatrix}. \tag{19}$$

Substituting (15) into (19) yields

$$\begin{aligned} \dot{\zeta}_1 &= \begin{bmatrix} \frac{1}{2}|s|^{-\frac{1}{2}} \left(-k_1 \mathrm{sig}^{1/2}(s) - \bar{k}_2 \mathrm{sig}^{r}(s) + g\right) \\ -k_3 \mathrm{sign}(s) + \dot{f}(t) \end{bmatrix} \\ &= |s|^{-\frac{1}{2}} \begin{bmatrix} \left(-\frac{k_1}{2} \mathrm{sig}^{1/2}(s) - \frac{\bar{k}_2}{2} \mathrm{sig}^{r}(s) + \frac{g}{2}\right) \\ \mathrm{sig}^{1/2}(s) \left(-k_3 + \dot{f}(t) \mathrm{sign}(s)\right) \end{bmatrix} \\ &= |s|^{-\frac{1}{2}} A_1 \zeta_1 \end{aligned} \tag{20}$$

$$\begin{aligned} \dot{\zeta}_2 &= \begin{bmatrix} r|s|^{r-1} \left(-k_1 \mathrm{sig}^{1/2}(s) - \bar{k}_2 \mathrm{sig}^{r}(s) + g\right) \\ -k_3 \mathrm{sign}(s) + \dot{f}(t) \end{bmatrix} \\ &= |s|^{r-1} \begin{bmatrix} -r k_1 \mathrm{sig}^{1/2}(s) - r \bar{k}_2 \mathrm{sig}^{r}(s) + r g \\ \mathrm{sig}^{1-r}(s) \left(-k_3 + \dot{f}(t) \mathrm{sign}(s)\right) \end{bmatrix} \\ &= |s|^{r-1} A_2 \zeta_2 \end{aligned} \tag{21}$$

where

$$\begin{aligned} A_1 &= \begin{bmatrix} -\frac{k_1}{2} - \frac{k_2}{2}|s|^{r-\frac{1}{2}} & \frac{1}{2} \\ -k_3 + \dot{f}(t) \mathrm{sign}(s) & 0 \end{bmatrix} \\ A_2 &= \begin{bmatrix} -r k_1 |s|^{\frac{1}{2}-r} - r k_2 & r \\ |s|^{1-2r} \left(-k_3 + \dot{f}(t) \mathrm{sign}(s)\right) & 0 \end{bmatrix}. \end{aligned} \tag{22}$$

Taking the derivative of Lyapunov function (16), then

$$\begin{aligned} \dot{V} &= \dot{V}_1 + \dot{V}_2 \\ &= \dot{\zeta}_1^{\mathrm{T}} H_1 \zeta_1 + \zeta_1^{\mathrm{T}} H_1 \dot{\zeta}_1 + \dot{\zeta}_2^{\mathrm{T}} H_2 \zeta_2 + \zeta_2^{\mathrm{T}} H_2 \dot{\zeta}_2 \\ &= |s|^{-\frac{1}{2}} \zeta_1^{\mathrm{T}} \left[A_1^{\mathrm{T}} H_1 + H_1 A_1\right] \zeta_1 \\ &\quad + |s|^{r-1} \zeta_2^{\mathrm{T}} \left[A_2^{\mathrm{T}} H_2 + H_2 A_2\right] \zeta_2. \end{aligned} \tag{23}$$

The matrices A_1 and A_2 are Hurwitz if and only if $k_1 > 0$, $\bar{k}_2 > 0$, $k_3 > |\dot{f}(t)|$. Under the condition that H_1 and H_2 are positive definite, there exists matrices $\Pi_1 > 0$, $\Pi_2 > 0$ such that

$$\begin{aligned} A_1^{\mathrm{T}} H_1 + H_1 A_1 &= -\Pi_1 \\ A_2^{\mathrm{T}} H_2 + H_2 A_2 &= -\Pi_2. \end{aligned} \tag{24}$$

Substituting (24) into (23)

$$\dot{V} = -|s|^{-\frac{1}{2}} \zeta_1^{\mathrm{T}} \Pi_1 \zeta_1 - |s|^{r-1} \zeta_2^{\mathrm{T}} \Pi_2 \zeta_2. \tag{25}$$

Meanwhile, the following Rayleigh's inequality can be acquired as:

$$\begin{aligned} \rho_{\min}\left\{\Pi_1\right\} \left\|\zeta_1\right\|^2 \le \zeta_1^{\mathrm{T}} \Pi_1 \zeta_1 \le \rho_{\max}\left\{\Pi_1\right\} \left\|\zeta_1\right\|^2 \\ \rho_{\min}\left\{\Pi_2\right\} \left\|\zeta_2\right\|^2 \le \zeta_2^{\mathrm{T}} \Pi_2 \zeta_2 \le \rho_{\max}\left\{\Pi_2\right\} \left\|\zeta_2\right\|^2 \end{aligned} \tag{26}$$

where $\rho_{\min}\{\Pi_1\}$, $\rho_{\min}\{\Pi_2\}$ and $\rho_{\max}\{\Pi_1\}$, $\rho_{\max}\{\Pi_2\}$ denote minimum and maximum eigenvalues of matrix Π_1, Π_2, respectively.

Consequently, based on Rayleigh's inequality (18), (26) and subsequent inequality

$$\begin{aligned} |s|^{\frac{1}{2}} \le \|\zeta_1\| \le \frac{V_1^{1/2}}{\rho_{\min}^{1/2}\left\{H_1\right\}} \le \frac{V^{1/2}}{\rho_{\min}^{1/2}\left\{H_1\right\}} \\ \Rightarrow |s|^{-\frac{1}{2}} \ge \frac{\rho_{\min}^{1/2}\left\{H_1\right\}}{V_1^{1/2}} \ge \frac{\rho_{\min}^{1/2}\left\{H_1\right\}}{V^{1/2}} \\ |s|^{r} \le \|\zeta_2\| \le \frac{V_2^{1/2}}{\rho_{\min}^{1/2}\left\{H_2\right\}} \le \frac{V^{1/2}}{\rho_{\min}^{1/2}\left\{H_2\right\}} \end{aligned}$$

$$\Rightarrow |s|^{r-1} \geq \frac{V_2^{\frac{r-1}{2r}}}{\rho_{\min}^{\frac{r-1}{2r}}\{H_2\}} \geq \frac{V^{\frac{r-1}{2r}}}{\rho_{\min}^{\frac{r-1}{2r}}\{H_2\}}, \ (0<r<1)$$

when $s \in [1, \infty]$, then $r > 1$. $\dot{V}$ can be rewritten as

$$\begin{aligned}
\dot{V} \leq & -|s|^{-\frac{1}{2}}\rho_{\min}\{\Pi_1\}\|\zeta_1\|^2 - |s|^{r-1}\rho_{\min}\{\Pi_2\}\|\zeta_2\|^2 \\
\leq & -|s|^{-\frac{1}{2}}\left(\rho_{\min}\{\Pi_1\}\|\zeta_1\|^2 + \rho_{\min}\{\Pi_2\}\|\zeta_2\|^2\right) \\
\leq & -\frac{\rho_{\min}^{1/2}\{H_1\}}{V^{1/2}}\left(\frac{\rho_{\min}\{\Pi_1\}}{\rho_{\max}\{H_1\}}V_1 + \frac{\rho_{\min}\{\Pi_2\}}{\rho_{\max}\{H_2\}}V_2\right) \\
\leq & -\frac{\rho_{\min}^{1/2}\{H_1\}\rho_{\min}\{\Pi_1\}}{\rho_{\max}\{H_1\}}V_1V^{-1/2} \\
& -\frac{\rho_{\min}^{1/2}\{H_1\}\rho_{\min}\{\Pi_2\}}{\rho_{\max}\{H_2\}}V_2V^{-1/2} \\
\leq & -\mu_1(V_1+V_2)V^{-1/2} = -\mu_1V^{1/2}
\end{aligned} \tag{27}$$

where $\mu_1 = \{\frac{\rho_{\min}^{1/2}\{H_1\}\rho_{\min}\{\Pi_1\}}{\rho_{\max}\{H_1\}}, \frac{\rho_{\min}^{1/2}\{H_1\}\rho_{\min}\{\Pi_2\}}{\rho_{\max}\{H_2\}}\}$.

when $s \in [0, 1]$, then $0 < r < 1$. $\dot{V}$ can be rewritten as

$$\begin{aligned}
\dot{V} \leq & -|s|^{-1/2}\rho_{\min}\{\Pi_1\}\|\zeta_1\|^2 - |s|^{r-1}\rho_{\min}\{\Pi_2\}\|\zeta_2\|^2 \\
\leq & -\frac{\rho_{\min}^{1/2}\{H_1\}\rho_{\min}\{\Pi_1\}}{\rho_{\max}\{H_1\}}V^{\frac{1}{2}} \\
& -\frac{\rho_{\min}^{\frac{1-r}{2r}}\{H_2\}\rho_{\min}\{\Pi_2\}}{\rho_{\max}\{H_2\}}V^{\frac{3r-1}{2r}} \\
\leq & -\mu_2V^{\frac{1}{2}} - \mu_3V^{\frac{3r-1}{2r}}
\end{aligned} \tag{28}$$

where $\mu_2 = \frac{\rho_{\min}^{1/2}\{H_1\}\rho_{\min}\{\Pi_1\}}{\rho_{\max}\{H_1\}}$, $\mu_3 = \frac{\rho_{\min}^{\frac{1-r}{2r}}\{H_2\}\rho_{\min}\{\Pi_2\}}{\rho_{\max}\{H_2\}}$.

According to the chosen Lyapunov function (16), it can be verified that the system state s and g can convergence to origin in finite-time from (27) and (28).

E. Parameter Analysis and Design Guidelines

To ensure optimal parameters, the impact of control parameters on system performance is analyzed and discussed. The proposed sliding mode controller consists of the current penalty function $1/\delta(\kappa)$, the nonsingular integral sliding mode surface (11), and the VRST control law (10). The impact of control parameters on system performance is as follows.

1) For the parameters of current penalty function $1/\delta(\kappa)$. The ς is usually determined by the rated current. For the parameter η, if the value of η is too larger, the q-axis current will be overconstraint and the transient performance will be affected. The value of ε is designed to be just less than 1, it determines the severity of the penalty, and the closer ε is to 1, the greater the severity of the current constraints.
2) In the sliding mode surface, the larger the value of λ_0, the faster the convergence speed, while excessive λ_0 will bring overshoot and increase control output. The λ_1 plays an important role in improving control accuracy, eliminating steady-state errors and enhancing system robustness. However, unreasonable increase in the value of λ_1 can lead to significant overshoot. In the proposed control law, the convergence speed of reaching law is mainly determined by k_1, k_2. The larger the value of k_1, k_2, the faster the convergence speed. However, if the k_1 is too large, the chattering will be increased, and excessive k_2 causes significant overshoot. In addition, the c_1 will affect the change rate of $\bar{k}_2$. Similarly, the choice of r_1 will also affect the convergence speed and overshoot of the system.

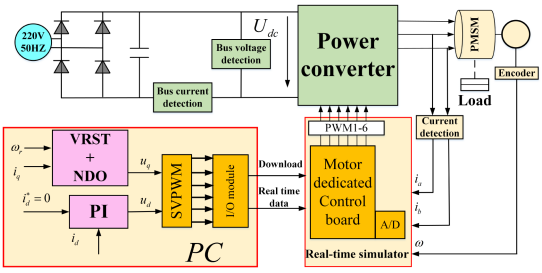

Fig. 4. Internal schematic diagram of experimental platform.

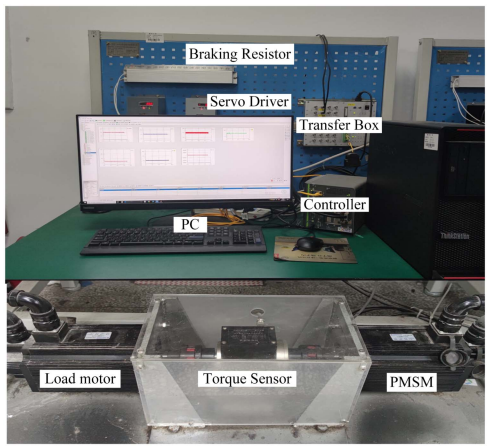

Fig. 5. Photo of experimental platform.

V. Experiments Validation

In this section, to verify the effectiveness and superiority of the proposed control strategy, the experiments in different conditions are constructed based on the motor platform. The internal structure diagram and photograph of the experimental platform are revealed in Figs. 4 and 5, respectively. The experimental platform consists of a 130MB 150 A surface-mounted PMSM coupled with the load motor. It also includes a power converter based on insulated gate bipolar transistor, and the LINKS-RT rapid prototyping system as the controller. A single-phase uncontrollable rectifier circuit is used to provide the dc bus voltage. The switching frequency is set as 10 kHz. Table I shows the nominal parameters of the PMSM.

The experiment mainly includes five parts as follows.

1) Comparative verification of transient performance during startup.
2) Antidisturbance performance with sudden load torque.

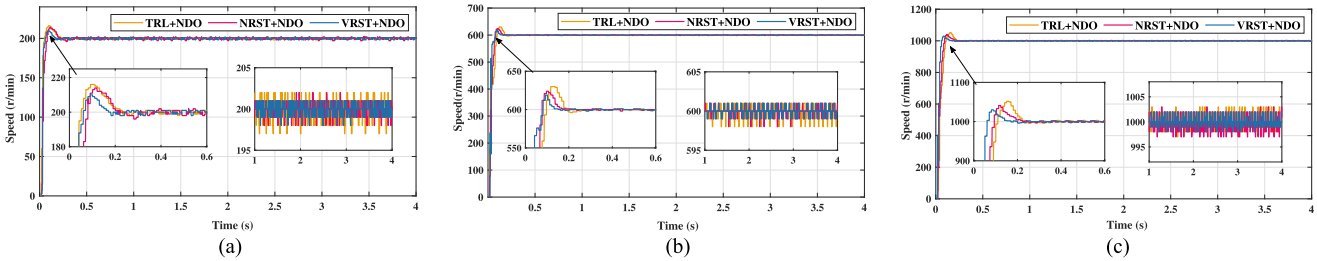

Fig. 6. Speed response curves of the motor starting stage. (a) 200 r/min. (b) 600 r/min. (c) 1000 r/min.

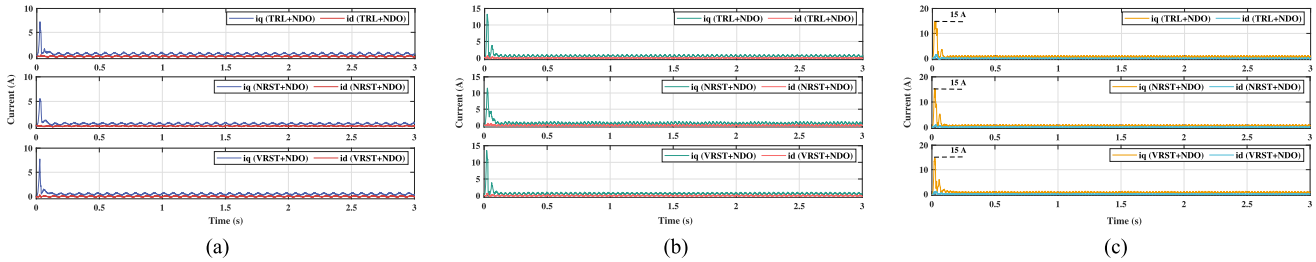

Fig. 7. *D-q* axis curves of the motor starting stage. (a) 200 r/min. (b) 600 r/min. (c) 1000 r/min.

TABLE I
NOMINAL PARAMETERS OF PMSM

Parameters name	Symbol	Value and unit
Rated power	P_N	1.5 kW
Rated speed	n_N	1000r/ min
Stator inductance in *d*-axis	L_{d}	6.65 mH
Stator inductance in *q*-axis	L_{q}	6.65 mH
Stator resistance	R_{s}	1.84 Ω
Rotor magnetic flux	Φ	0.32 Wb

3) Transient performance in stepped acceleration and deceleration.
4) Robustness experiment under parameters variations.
5) Suppress performance for periodic harmonic disturbances with the proposed NDO.

A. Experiment 1

In this experiment, it is compared with the terminal reaching law (TRL) combines with the NDO (TRL+NDO), the novel robust supertwisting (NRST) reaching law combines with the NDO (NRST+NDO), respectively.

In TRL+NDO, (11) and (29) are selected as the sliding mode surface and the reaching law, respectively. The sliding mode speed controller u_{q1} with single-loop structure can be derived as (30)

$$\dot{s} = -m_1|s|^{r_2}\mathrm{sign}(s) - m_2 s \tag{29}$$

$$u_{q1} = -\frac{1}{b}\begin{bmatrix} a(x) + \dot{d}_f + \frac{\lambda_0}{\delta(\kappa)}(x_2 + d_f) \\ +\lambda_1 \mathrm{sig}^p(x_1) + m_1|s|^{r_2}\mathrm{sign}(s) + m_2 s \end{bmatrix} \tag{30}$$

where $m_1 > 0, m_2 > 0, 0 < r_2 < 1$.

In NRST+NDO, (11) is also selected as the sliding mode surface. Besides, the NRST in [42] is presented as (31). The corresponding controller can be derived as (32)

$$\begin{aligned} \dot{s} &= -m_3|s|^{1/2}\mathrm{sign}(s) - m_4 s + v \\ \dot{v} &= -m_5\mathrm{sign}(s) - m_6 s \end{aligned} \tag{31}$$

$$u_{q2} = -\frac{1}{b}\begin{bmatrix} a(x) + \dot{d}_f + \frac{\lambda_0}{\delta(\kappa)}(x_2 + d_f) - v \\ +\lambda_1 \mathrm{sig}^p(x_1) + m_3|s|^{1/2}\mathrm{sign}(s) + m_4 s \end{bmatrix} \tag{32}$$

where $m_3 > 0, m_4 > 0, m_5 > 0, m_6 > 0$.

To ensure the fairness of the experiment and the credibility of the results, the parameters in the d-axis current PI controller are selected as $K_{\mathrm{p}} = 9$, $K_{\mathrm{i}} = 100$ among above-mentioned three control strategies. The other control parameters are shown in the Table II.

First, the control performance with three control strategies is tested under different given speeds. The given speeds are selected as 200, 600, and 1000 r/min, respectively. The initial load torque is 0.5 Nm. The speed tracking curves of different control strategies are shown in Fig. 6. When the given test speed is 200 r/min, the overshoots under TRL+NDO, NRST+NDO,

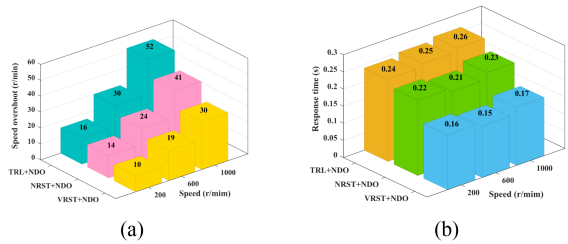

Fig. 8. Comparison of overshoot and response time during startup. (a) Overshoot. (b) Response time.

TABLE II
PARAMETERS OF THE CONTROLLER AND OBSERVER IN THREE CONTROL STRATEGIES

Control strategy	Controller	Observer
TRL+NDO	$\lambda_0 = 15, \lambda_1 = 56050, p = 1.2, r_2 = 0.9,$ $m_1 = 35, m_2 = 29, \varsigma = 15, \eta = 2.8, \varepsilon = 0.98$	$\alpha_{1,3,5} = 0.97, \alpha_{2,4,6} = 0.95, l_1 = 42, l_2 = 401,$ $l_3 = 46, l_4 = 411, l_5 = 55, l_6 = 613$
NRST+NDO	$\lambda_0 = 15, \lambda_1 = 56050, p = 1.2, m_3 = 55, m_4 = 31,$ $m_5 = 119, m_6 = 106, \varsigma = 15, \eta = 3, \varepsilon = 0.02$	$\alpha_{1,3,5} = 0.97, \alpha_{2,4,6} = 0.95, l_1 = 43, l_2 = 405,$ $l_3 = 44, l_4 = 413, l_5 = 54, l_6 = 616$
VRST+NDO	$\lambda_0 = 15, \lambda_1 = 56050, p = 1.2, k_1 = 55, k_2 = 6, k_3 = 119,$ $c_1 = 1.1, r_1 = 0.1, \varsigma = 15, \eta = 2.7, \varepsilon = 0.15$	$\alpha_{1,3,5} = 0.97, \alpha_{2,4,6} = 0.95, l_1 = 42, l_2 = 403,$ $l_3 = 45, l_4 = 410, l_5 = 55, l_6 = 613$

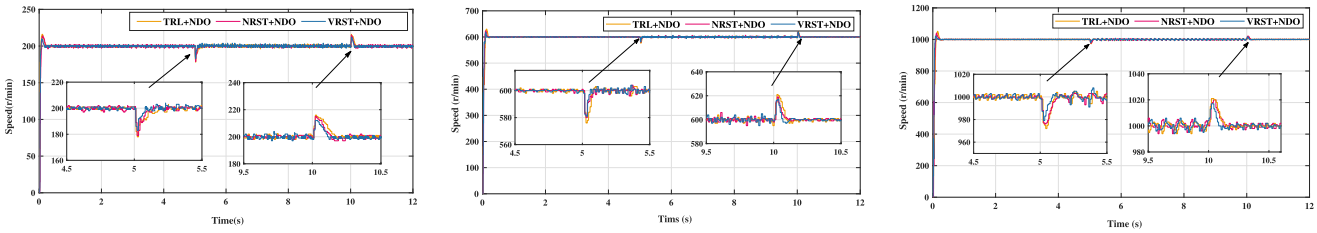

Fig. 9. Speed response curves with load disturbance. (a) 200 r/min. (b) 600 r/min. (c) 1000 r/min.

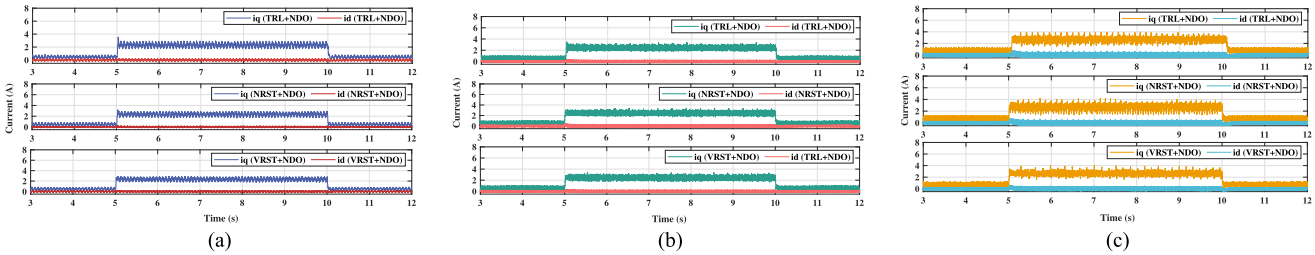

Fig. 10. *D-q* axis curves with load disturbance. (a) 200 r/min. (b) 600 r/min. (c) 1000 r/min.

and the proposed VRST+NDO are 16, 14, and 10 r/min, respectively. The response time is around 0.24, 0.22, and 0.16 s, respectively. The comparison of response time and speed overshoot with three control strategies under different given speeds are shown in Fig. 8. The comparative results indicate that the proposed VRST+NDO has shorter response time and smaller overshoot. Besides, the *d-q* axis current curves at three control strategies under different given speeds are shown in Fig. 7, As seen in Fig. 7(c), the maximum current of *q*-axis is limited at 15 A.

B. Experiment 2

To verify the robustness of the proposed control scheme under sudden load torque, the following antidisturbance experiments will be tested. After the motor reaches the expected speed and runs stably, the external disturbance of 3.5 Nm is abruptly added at t = 5 s, and it is removed when t = 10 s. The load torque as an external disturbance is provided by the load motor, which is linked to the PMSM via a torque sensor to apply a constant torque. The speed response curves of three control strategies are shown in Fig. 9. When the motor runs stably at 600 r/min. The speed drop with adding the external disturbances under TRL+NDO, NRST+NDO, and the proposed VRST+NDO is 24, 20, and 19 r/min, respectively. The adjustment time is around 0.13, 0.11, and 0.07 s, respectively. The speed rise with removing the external disturbances is 21, 19, and 17 r/min, respectively. The adjustment time is around 0.19, 0.15, and 0.12 s, respectively. The *d-q* axis current curves under sudden load disturbance are shown in Fig. 10. After the load torque disturbance is added and removed, the adjustment time to reach steady-state again in different speeds is shown in Fig. 12. The comparison results of speed fluctuation are shown in Fig. 13, the lower part shows the speed drop of three methods when the load disturbance is suddenly applied at t = 5 s, the upper part shows the speed rise of three methods when the load disturbance is suddenly removed at t = 10 s. The comparative results show that the proposed VRST+NDO has the shortest adjustment time and the smallest speed fluctuation under load torque disturbance.

In addition, the estimated waveforms of $\hat{d}$, $\hat{d}_{\mathrm{h1}}$, $\hat{d}_{\mathrm{h2}}$, and the lumped disturbances $d_f = \hat{d} + \hat{d}_{\mathrm{h1}} + \hat{d}_{\mathrm{h2}}$ by the NDO are shown in Fig. 11, respectively. It is worth noting that the estimated aperiodic disturbances have a certain initial value due to friction and no-load torque. Moreover, the higher the angular velocity, the greater the estimated aperiodic disturbance $\hat{d}$. For estimated periodic disturbances, the results show that

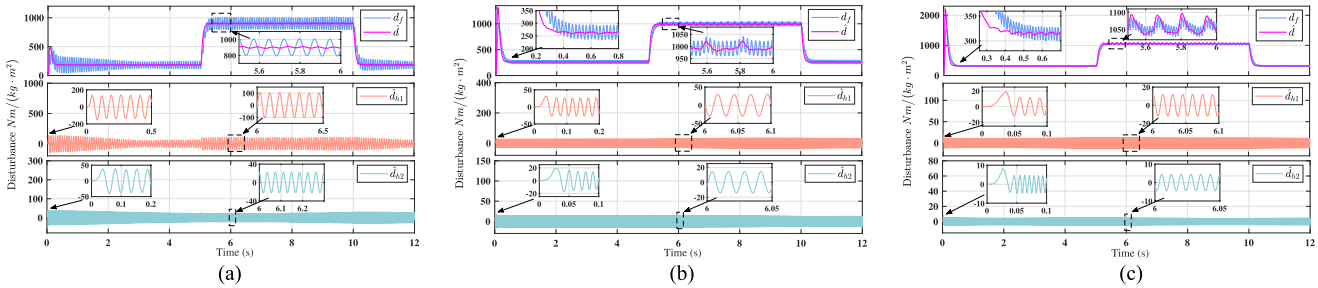

Fig. 11. Disturbance waveforms estimated by the NDO. (a) 200 r/min. (b) 600 r/min. (c) 1000 r/min.

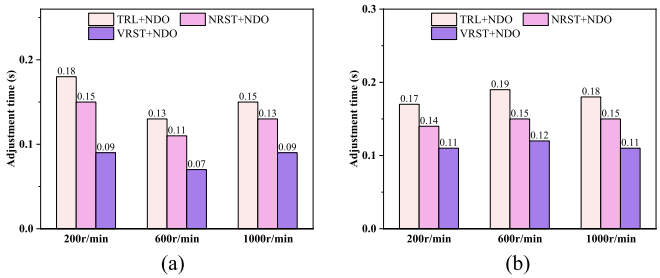

Fig. 12. Comparison of adjustment time under sudden load torque disturbance. (a) Loading. (b) Unloading.

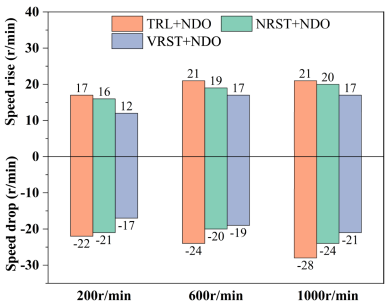

Fig. 13. Comparison of speed fluctuation under sudden load torque.

the amplitude of periodic harmonic disturbance decreases with increasing velocity. Therefore, harmonic disturbances at high speeds can be ignored.

C. Experiment 3

To satisfy the actual control requirements, the control performance of the proposed control strategy in stepped acceleration and deceleration will be verified in this section. First, the motor runs stably at 200 r/min, then the speed increases by 400 r at 4 and 8 s, respectively. The experimental result with acceleration is shown in Fig. 14(a). Similarly, the motor runs stably at 1000 r/min, then the speed decreases by 400 r at 4 and 8 s, respectively. The experimental result with deceleration is shown in Fig. 14(b). It can be seen that the proposed VRST-NDO has fast and smooth speed regulation performance.

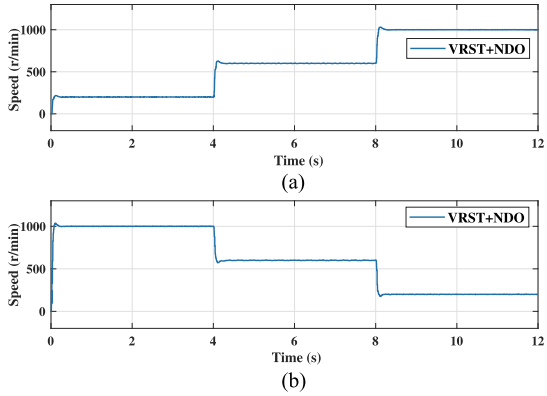

Fig. 14. Speed curves under acceleration and deceleration. (a) Acceleration. (b) Deceleration.

D. Experiment 4

Due to the influence of working environment, the parameters of the motor may change during actual operation. To verify the robustness with mismatched parameters, experimental verification is completed by changing the relevant parameters in the controller, such as Φ, L_s, R_s. First, when the motor runs stably at 600 r/min, the initial value of the rotor flux Φ is changed by $\pm 20\%$ at t = 5 s. Fig. 15(a) shows the speed fluctuation curve under changes in rotor flux. The results show that when the rotor flux is increased by 20%, the speed fluctuation is around 40 r/min, and the recovery time is around t = 0.21 s. When the rotor flux Φ is decreased by 20%, the speed fluctuation is around 30 r/min, and the recovery time is about t = 0.09 s. It can be seen that the change of rotor flux Φ will have a significant impact on the stable operation of the motor, but the controller can respond quickly, and the speed can return to the expected speed in a very short period of time.

Second, when the motor runs stably at 600 r/min, the initial value of the stator resistance R_s is changed by $\pm 50\%$ at t = 5 s. Fig. 15(b) shows the speed fluctuation curves under the change of stator resistance R_s. The results show that no matter when the stator resistance is increased by 50% or decreased by 50%, the speed curves have no significant change.

Finally, when the motor runs stably at 600 r/min, the initial value of the stator inductance L_s is changed by $\pm 50\%$ at t = 5 s. The speed fluctuation curves are shown in Fig. 15(c). The results

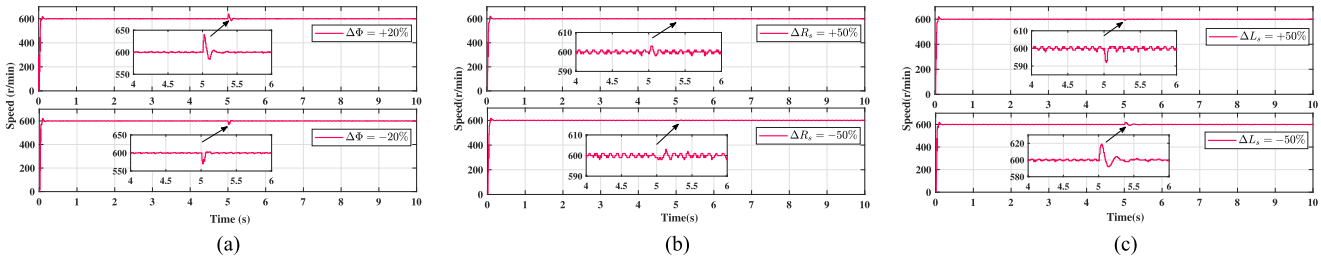

Fig. 15. Speed fluctuation curves under parameter variations. (a) Rotor flux. (b) Stator resistance. (c) Stator inductance.

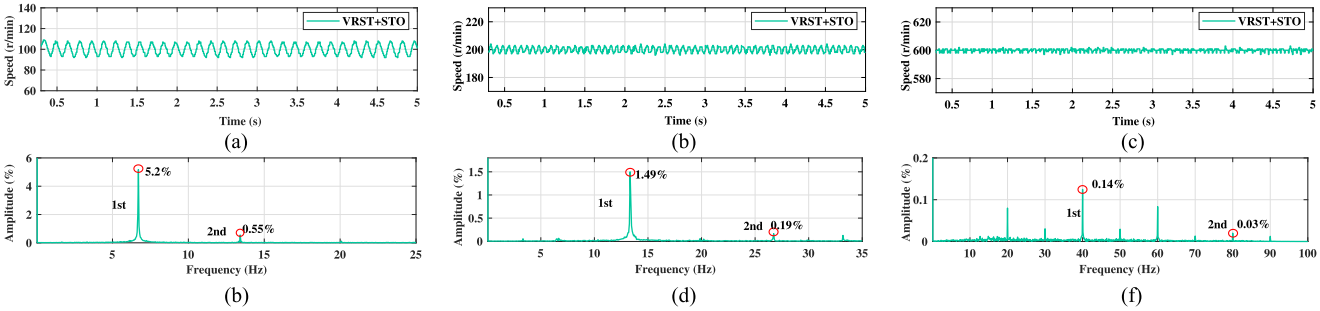

Fig. 16. Steady-state performance of VRST+STO. (a) Speed waveform at 100 r/min. (b) Fourier analysis at 100 r/min. (c) Speed waveform at 200 r/min. (d) Fourier analysis at 200 r/min. (e) Speed waveform at 600 r/min. (f) Fourier analysis at 600 r/min.

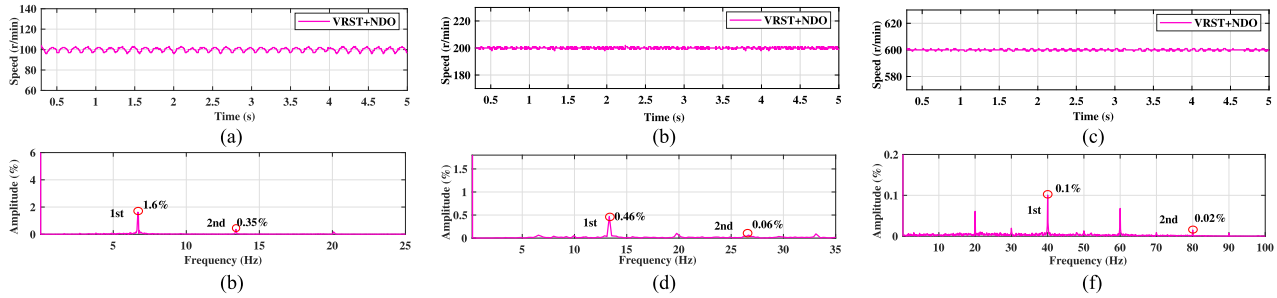

Fig. 17. Steady-state performance of VRST+NDO control strategy. (a) Speed waveform at 100 r/min. (b) Fourier analysis at 100 r/min. (c) Speed waveform at 200 r/min. (d) Fourier analysis at 200 r/min. (e) Speed waveform at 600 r/min. (f) Fourier analysis at 600 r/min.

show that when the stator inductance L_s is increased by 50%, the speed fluctuation is about 8 r/min, and the recovery time is around t = 0.08 s. when the stator inductance L_s is decreased by 50%, the speed fluctuation is about 19 r/min, and the recovery time is around t = 0.30 s. In summary, the proposed control strategy VRST+NDO has strong robustness under parameter variations.

E. Experiment 5

To verify the harmonic suppression performance of the proposed NDO, the speed tracking accuracy between the VRST controller combined with the supertwisting disturbance observer [43] (VRST+STO) and the proposed control strategy of VRST+NDO will be compared. Subsequently, the Fourier analysis of the steady-state speed will be completed. The speed waveforms of 100, 200, and 600 r/min with VRST+STO control strategy are shown in Fig. 16(a), (c), and (e), respectively. For 100 r/min, Fig. 16(b) shows that the first (6.67 Hz) and the second (13.33 Hz) harmonic is 5.2% and 0.55%, respectively. For 200 r/min, Fig. 16(d) shows that the first (13.33 Hz) and the second (26.67 Hz) harmonic is 1.49% and 0.19%, respectively. For 600 r/min, Fig. 16(f) shows that the first (40 Hz) and the second (80 Hz) harmonic is 0.14% and 0.03%, respectively. The speed waveforms of 100, 200, and 600 r/min under VRST+NDO control strategy are shown in Fig. 17(a), (c), and (e), respectively. For 100 r/min, Fig. 17(b) shows that the first (6.67 Hz) and the second (13.33 Hz) harmonic is 1.6% and 0.35%, respectively. For 200 r/min, Fig. 17(d) shows that the first (13.33 Hz) and the second (26.67 Hz) harmonic is 0.46% and 0.06%, respectively. For 600 r/min, Fig. 17(f) shows that the first (40 Hz) and the second (80 Hz) harmonic is 0.1% and 0.02%, respectively. The results show that the first and second harmonics are effectively reduced under the action of the NDO, the designed composite controller has excellent speed tracking accuracy.

VI. Conclusion

In this article, a VRST sliding mode single-loop control strategy based on NDO is proposed to improve the speed control performance of PMSM. In addition, considering the overcurrent protection in a single-loop control structure, an improved q-axis current penalty function is embedded in the controller to better balance current protection and dynamic performance. Finally, a series of experiments are conducted on an RT-SIM surface-mounted PMSM experimental platform. The experimental results demonstrate that the proposed VRST+NDO composite control strategy not only exhibits fast transient response, small overshoot, exceptional robustness against load torque and parameter mismatch, but also has a good overcurrent protection effect. Besides, the first and second harmonic disturbances can be effectively suppressed by NDO, thus, the speed fluctuation is reduced, and the control accuracy is improved.

References

[1] D. Zhang et al., "A PMSM control system for electric vehicle using improved exponential reaching law and proportional resonance theory," *IEEE Trans. Veh. Technol.*, vol. 72, no. 7, pp. 8566–8578, Jul. 2023.

[2] I. Zamudio-Ramírez, J. A. Antonino-Daviu, M. Trejo-Hernandez, and R. A. Osornio-Rios, "Cutting tool wear monitoring in CNC machines based in spindle-motor stray flux signals," *IEEE Trans. Ind. Informat.*, vol. 18, no. 5, pp. 3267–3275, May 2022.

[3] Y. Wang, S. Fang, and J. Hu, "Active disturbance rejection control based on deep reinforcement learning of PMSM for more electric aircraft," *IEEE Trans. Power Electron.*, vol. 38, no. 1, pp. 406–416, Jan. 2023.

[4] S. Zhou et al., "A robust encoderless control for PMSM drives: A revised hybrid active flux-based technique," *IEEE Trans. Power Electron.*, vol. 38, no. 11, pp. 14438–14449, Nov. 2023.

[5] H. Cao et al., "Improved ADRC with a cascade extended state observer based on quasi-generalized integrator for PMSM current disturbances attenuation," *IEEE Trans. Transp. Electrif.*, vol. 10, no. 1, pp. 2145–2157, Mar. 2024.

[6] X. Song, H. Wang, X. Ma, X. Yuan, and X. Wu, "Robust model predictive current control for a nine-phase open-end winding PMSM with high computational efficiency," *IEEE Trans. Power Electron.*, vol. 38, no. 11, pp. 13933–13943, Nov. 2023.

[7] J. Gu, S. You, W. Kim, and J. Moon, "Fuzzy event-triggered super twisting sliding mode control for position tracking of permanent magnet synchronous motors under unknown disturbances," *IEEE Trans. Ind. Inform.*, vol. 19, no. 9, pp. 9843–9854, Sep. 2023.

[8] X. Yu, B. Zhou, L. Xiong, and S. Jiang, "Composite sliding mode speed control for sinusoidal doubly salient electromagnetic machine drives using fast reaching law and disturbance compensation," *IEEE Trans. Ind. Electron.*, vol. 70, no. 7, pp. 6563–6573, Jul. 2023.

[9] L. Zhang, Z. Chen, X. Yu, J. Yang, and S. Li, "Sliding-mode-based robust output regulation and its application in PMSM servo systems," *IEEE Trans. Ind. Electron.*, vol. 70, no. 2, pp. 1852–1860, Feb. 2023.

[10] Z. Zhang, X. Yang, W. Wang, K. Chen, N. C. Cheung, and J. Pan, "Enhanced sliding mode control for PMSM speed drive systems using a novel adaptive sliding mode reaching law based on exponential function," *IEEE Trans. Ind. Electron.*, vol. 71, no. 10, pp. 11978–11988, Oct. 2024.

[11] S. Huang, J. Wang, L. Xiong, J. Liu, P. Li, and Z. Wang, "Distributed predefined-time fractional-order sliding mode control for power system with prescribed tracking performance," *IEEE Trans. Power Syst.*, vol. 37, no. 3, pp. 2233–2246, May 2022.

[12] T. Wang, B. Wang, Y. Yu, and D. Xu, "High-order sliding-mode observer with adaptive gain for sensorless induction motor drives in the wide-speed range," *IEEE Trans. Ind. Electron.*, vol. 70, no. 11, pp. 11055–11066, Nov. 2023.

[13] G. P. Incremona, M. Rubagotti, M. Tanelli, and A. Ferrara, "A general framework for switched and variable gain higher order sliding mode control," *IEEE Trans. Autom. Control*, vol. 66, no. 4, pp. 1718–1724, Apr. 2021.

[14] X. Sun, J. Cao, G. Lei, Y. Guo, and J. Zhu, "A composite sliding mode control for SPMSM drives based on a new hybrid reaching law with disturbance compensation," *IEEE Trans. Transp. Electrif.*, vol. 7, no. 3, pp. 1427–1436, Sep. 2021.

[15] T. H. Nguyen, T. T. Nguyen, V. Q. Nguyen, K. M. Le, H. N. Tran, and J. W. Jeon, "An adaptive sliding-mode controller with a modified reduced-order proportional integral observer for speed regulation of a permanent magnet synchronous motor," *IEEE Trans. Ind. Electron.*, vol. 69, no. 7, pp. 7181–7191, Jul. 2022.

[16] I. Balogoun, S. Marx, T. Liard, and F. Plestan, "Super-twisting sliding mode control for the stabilization of a linear hyperbolic system," *IEEE Control Syst. Lett.*, vol. 7, pp. 1–6, 2023.

[17] N. Tiwary, V. Naik N., A. K. Panda, A. Narendra, and R. K. Lenka, "A robust voltage control of DAB converter with super-twisting sliding mode approach," *IEEE J. Emerg. Sel. Topics Ind. Electron.*, vol. 4, no. 1, pp. 288–298, Jan. 2023.

[18] Z. Zhen, C. Yu, S. Jiang, and J. Jiang, "Adaptive super-twisting control for automatic carrier landing of aircraft," *IEEE Trans. Aerosp. Electron. Syst.*, vol. 56, no. 2, pp. 984–997, Apr. 2020.

[19] Z. Zhang and X. Liu, "An improved super-twisting sliding mode single-loop control with current-constraint for PMSM based on two-time scale disturbance observer," *IEEE Trans. Transp. Electrif.*, vol. 10, no. 3, pp. 5389–5399, Sep. 2024.

[20] I. Nagesh and C. Edwards, "A multivariable super-twisting sliding mode approach," *Automatica*, vol. 50, no. 3, pp. 984–988, 2014.

[21] X. Liu and H. Yu, "Continuous adaptive integral-type sliding mode control based on disturbance observer for PMSM drives," *Nonlinear Dyn.*, vol. 104, pp. 1429–1441, 2021.

[22] L. Qu, W. Qiao, and L. Qu, "An extended-state-observer-based sliding-mode speed control for permanent-magnet synchronous motors," *IEEE J. Emerg. Sel. Topics Power Electron.*, vol. 9, no. 2, pp. 1605–1613, Apr. 2021.

[23] Z. Zhang, X. Liu, J. Yu, and H. Yu, "Time-varying disturbance observer based improved sliding mode single-loop control of PMSM drives with a hybrid reaching law," *IEEE Trans. Energy Convers.*, vol. 38, no. 4, pp. 2539–2549, Dec. 2023.

[24] L. Chen, H. Zhang, H. Wang, K. Shao, G. Wang, and A. Yazdani, "Continuous adaptive fast terminal sliding mode-based speed regulation control of PMSM drive via improved super- twisting observer," *IEEE Trans. Ind. Electron.*, vol. 71, no. 5, pp. 5105–5115, May 2024.

[25] B. Wang, M. Tian, Y. Yu, Q. Dong, and D. Xu, "Enhanced ADRC with quasi-resonant control for PMSM speed regulation considering aperiodic and periodic disturbances," *IEEE Trans. Transp. Electrif.*, vol. 8, no. 3, pp. 3568–3577, Sep. 2022.

[26] M. Tian, B. Wang, Y. Yu, Q. Dong, and D. Xu, "Discrete-time repetitive control-based ADRC for current loop disturbances suppression of PMSM drives," *IEEE Trans. Ind. Inform.*, vol. 18, no. 5, pp. 3138–3149, May 2022.

[27] G. Bi, G. Zhang, G. Wang, Q. Wang, Y. Hu, and D. Xu, "Adaptive iterative learning control-based rotor position harmonic error suppression method for sensorless PMSM drives," *IEEE Trans. Ind. Electron.*, vol. 69, no. 11, pp. 10870–10881, Nov. 2022.

[28] C. Zhao, Y. Zuo, H. Wang, and C. H. T. Lee, "Online-trained radial basis function neural network compensator for current harmonics suppression of electric drives," *IEEE Trans. Ind. Electron.*, pp. 1–11, 2024.

[29] T. Guo, Z. Sun, X. Wang, S. Li, and K. Zhang, "A simple current-constrained controller for permanent-magnet synchronous motor," *IEEE Trans. Ind. Inform.*, vol. 15, no. 3, pp. 1486–1495, Mar. 2019.

[30] C. Dai, T. Guo, J. Yang, and S. Li, "A disturbance observer-based current-constrained controller for speed regulation of PMSM systems subject to unmatched disturbances," *IEEE Trans. Ind. Electron.*, vol. 68, no. 1, pp. 767–775, Jan. 2021.

[31] Y. Wang, H. Yu, and Y. Liu, "Speed-current single-loop control with overcurrent protection for PMSM based on time-varying nonlinear disturbance observer," *IEEE Trans. Ind. Electron.*, vol. 69, no. 1, pp. 179–189, Jan. 2022.

[32] J. Zhang, W. Ren, and X.-M. Sun, "Current-constrained adaptive robust control for uncertain PMSM drive systems: Theory and experimentation," *IEEE Trans. Transp. Electrif.*, vol. 9, no. 3, pp. 4158–4169, Sep. 2023.

[33] Z. Zhou, C. Xia, Y. Yan, Z. Wang, and T. Shi, "Disturbances attenuation of permanent magnet synchronous motor drives using cascaded predictive-integral-resonant controllers," *IEEE Trans. Power Electron.*, vol. 33, no. 2, pp. 1514–1527, Feb. 2018.

[34] M. Tian, B. Wang, Y. Yu, Q. Dong, and D. Xu, "Robust adaptive resonant controller for PMSM speed regulation considering uncertain periodic and aperiodic disturbances," *IEEE Trans. Ind. Electron.*, vol. 70, no. 4, pp. 3362–3372, Apr. 2023.
[35] X. Meng, H. Yu, and J. Zhang, "An EPCH control strategy for complex nonlinear systems with actuator saturation and disturbances," *Inf. Sci.*, vol. 625, pp. 639–655, May 2023.
[36] H. Du, C. Qian, S. Yang, and S. Li, "Recursive design of finite-time convergent observers for a class of time-varying nonlinear systems," *Automatica*, vol. 49, no. 2, pp. 601–609, 2013.
[37] S. Huang, G. Li, H. Yu, X. Wang, S. Li, and Q. Li, "Composite-disturbance-observer-based backstepping control for three-phase inverters with multiple disturbances," *Control Eng. Pract.*, vol. 138, 2023, Art. no. 105599.
[38] C. Bai, Z. Yin, J. Luo, P. Luo, and J. Liu, "Robust composite finite-time convergent speed control of induction machine based on multiple sources disturbance estimation technology generalized proportional integral observer," *IEEE J. Emerg. Sel. Topics Power Electron.*, vol. 10, no. 5, pp. 6160–6170, Oct. 2022.
[39] P. Alinaghi Hosseinabadi, S. Mekhilef, H. R. Pota, and M. Kermadi, "Chattering-free fixed-time robust sliding mode controller for grid-connected inverters under parameter variations," *IEEE Trans. Emerg. Sel. Topics Power Electron.*, vol. 12, no. 1, pp. 579–592, Feb. 2024.
[40] J. Li, L. Zhang, L. Luo, and S. Li, "Extended state observer based current-constrained controller for a PMSM system in presence of disturbances: Design, analysis and experiments," *Control Eng. Pract.*, vol. 132, 2023, Art. no. 105412.
[41] M. J. Mirzaei, M. Asadollahi, E. Aslmostafa, and M. A. Badamchizadeh, "Continuous robust control based on fixed-time super-twisting disturbance observer," *IEEE Trans. Syst. Man Cybern. -Syst.*, vol. 54, no. 1, pp. 426–435, Jan. 2024.
[42] D. Fu, X. Zhao, and J. Zhu, "A novel robust super-twisting nonsingular terminal sliding mode controller for permanent magnet linear synchronous motors," *IEEE Trans. Power Electron.*, vol. 37, no. 3, pp. 2936–2945, Mar. 2022.
[43] Y.-C. Liu, S. Laghrouche, D. Depernet, A. Djerdir, and M. Cirrincione, "Disturbance-observer-based complementary sliding-mode speed control for PMSM drives: A super-twisting sliding-mode observer-based approach," *IEEE J. Emerg. Sel. Top. Power Electron.*, vol. 9, no. 5, pp. 5416–5428, Oct. 2021.

Yongzhi Chen received the B.S. degree in automation from the Nanjing University of Information Science and Technology, Nanjing, China, in 2022. He is currently working toward the M.S. degree in control engineering with Qingdao University, Qingdao, China.

His research interests include power electronics and motor drives.

Xudong Liu received the B.S. and M.S. degrees in automation from Qingdao University, Qingdao, China, in 2008 and 2011, respectively, and the Ph.D. degree in power electronics and electric drives from Shandong University, Jinan, China, in 2016.

He is currently a Distinguished Professor with the School of Automation, Qingdao University. His research interests include new energy systems, power electronics, and motor drive.